A Numerical Study on the Laminar Flow Field and Heat Transfer Coefficient Distribution for Supercritical Water in a Tube

Sang-Ho Lee†

Department of Mechanical Engineering, Wonkwang University, Cheonbuk 570-749, Korea

Key words: Thermodynamic critical point, Convective heat transfer, Pseudocritical temperature, Thermophysical properties, Zero gravity

ABSTRACT: Numerical analysis has been carried out to investigate laminar convective heat transfer at zero gravity in a tube for supercritical water near the thermodynamic critical point. Fluid flow and heat transfer are strongly coupled due to large variation of thermodynamic and transport properties such as density, specific heat, viscosity, and thermal conductivity near the critical point. Heat transfer characteristics in the developing region of the tube show transition behavior between liquid-like and gas-like phases with a peak in heat transfer coefficient distribution near the pseudocritical point. The peak of the heat transfer coefficient depends on pressure and wall heat flux rather than inlet temperature and Reynolds number. Results of the modeling provide convective heat transfer characteristics including velocity vectors, temperature, and the properties as well as the heat transfer coefficient. The effect of proximity on the critical point is considered and a heat transfer correlation is suggested for the peak of Nusselt number in the tube.

Nomenclature

A : tube area [m]
C_p : specific heat [J/kg·K]
D : tube diameter [m]
G : mass flux [kg/m^2·s]
Gr : Grashof number
h : heat transfer coefficient [W/m^2·K]
I : enthalpy [J/kg]
I_b : bulk fluid enthalpy [J/kg]
I_c : critical enthalpy [J/kg]
k : thermal conductivity [W/m·K]
L : tube length [m]
Nu : Nusselt number, hD/k_b
P : pressure [N/m^2]
Pe : Peclet number
P_R : reduced pressure, P/P_c
Q : heat flux [W/m^2]
R : tube radius [m]
r : radial coordinate [m]
Re : Reynolds number, $\rho uD/\mu$
T : temperature [K]
T_b : bulk fluid temperature, $(\int_A \rho u C_p T dA / \int_A \rho u C_p dA)$ [K]
T_{pc} : pseudocritical temperature [K]
T_R : reduced temperature, T/T_c
T^* : nondimensionalized temperature, $k_{in}(T-T_{in})/Q_w \cdot D$
u : axial velocity [m/s]
u_{in} : inlet velocity [m/s]
V : velocity vector [m/s]
v : radial velocity [m/s]
z : axial coordinate [m]

† Corresponding author
Tel.: +82-63-850-6683; fax: +82-63-850-6691
E-mail address: lsheagle@wonkwang.ac.kr

Greek symbols

β : compressibility [1/K]
μ : viscosity [kg/s·m]
θ : circumferential direction
ρ : density [kg/m^3]
τ : shear stress [N/m^2]
Φ : dissipation rate [J/kg·m^2]

Subscripts

b : bulk
c : critical point
fd : fully developed
in : inlet
pc : pseudocritical point
peak : maximum
w : tube wall

1. Introduction

Over the past years supercritical fluids have been used in many application areas including heat exchanger equipments in power plants, superconducting systems, and environmental extraction. Near the thermodynamic critical point there is no distinction between liquid and gas, and the supercritical fluids show transition behavior of molecular structure from liquid-like to gas-like phase across the pseudocritical point as temperature increases. With large variation of the thermodynamic and transport properties characteristics of fluid flow and heat transfer in this region are quite different from those of the constant property case.

Figure 1 shows the thermophysical properties variation of water for several pressures near the critical point. Density and viscosity decrease with the increase of temperature and the variations become steeper as the pressure approaches to the critical point. There are some peaks in specific heat and thermal conductivity while those of thermal conductivity are relatively small, and these peaks increase rapidly near the critical pressure. With the increase of pressure the pseudocritical temperature at which there is a peak in specific heat increases. These properties are coupled with momentum and heat transfer in the fluid flow through the thermodynamic state variables of temperature and pressure. Hence the convective heat transfer near the critical region is largely affected by the properties variation.

A lot of experimental and theoretical studies[2-19] have been carried out to investigate heat transfer phenomena for supercritical fluids because of a large number of industrial applications since 1950. Extensive data and various types of heat transfer correlations[2,3] were provided with theoretical analyses. And since the 1970's numerical methods have been used widely in many theoretical studies[5-9] because of

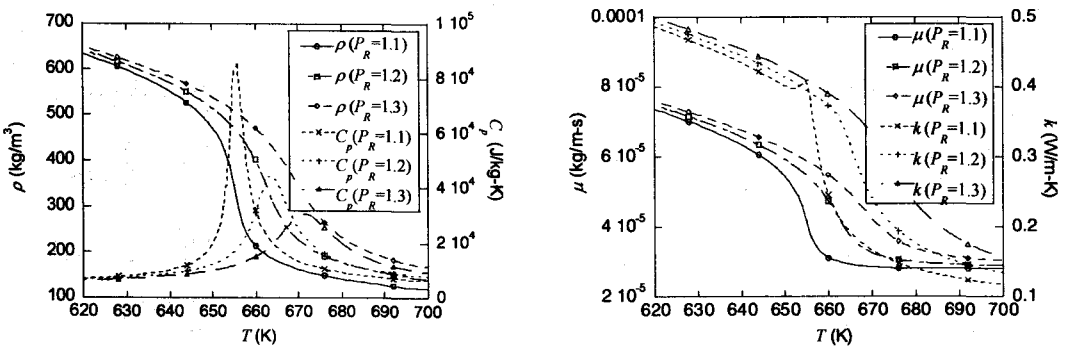

(a) Density and specific heat (b) Viscosity and thermal conductivity

Fig. 1 Thermophysical properties variation of water near the thermodynamic critical point.

difficulties in getting experimental data due to uncommon thermodynamic conditions of high pressure and temperature or cryogenic state.

Recently Choi et al.[5,6] investigated turbulent convective heat transfer characteristics of Nusselt number and friction factor for supercritical carbon dioxide in a straight duct with a square cross section and suggested several heat transfer correlations based on the typical Dittus and Boelter equation. Li et al.[7] predicted convective heat transfer characteristics for various wall temperatures and pressures in a heated curved pipe under the conditions of mixed convection. Lee and Howell[8] analyzed buoyancy effect in a vertical tube and compared simulation results from several turbulent Prandtl number models. Zhou and Krishnan[9] predicted laminar and turbulent heat transfer for channel flow of carbon dioxide near the critical point and compared their results with experimental data.

Kurganov and Kaptilnyi[10] experimentally analyzed shear stress and heat transfer coefficient in a vertical tube and suggested that heat transfer deterioration in heat transfer with the development of a peak in tube wall temperature is attributable to velocity profiles and shear stress distributions with reduced turbulence generation. Olson[11] examined overall heat transfer characteristics in a dual-pipe heat exchanger system which uses supercritical carbon dioxide and subcooled water. Ghajar and Asadi[12] suggested heat transfer correlation of Dittus-Boelter type with property ratios to account for large variations of thermophysical properties in the near-critical region.

Most of the experimental and theoretical investigations for fluid flow and heat transfer near the critical region are for turbulent flow because of the need for the design of practical systems. Despite several studies of laminar flow in the tube for supercritical fluids experimental data are sparse, and the effects of properties variation on heat transfer and fluid flow are still not well understood because of the large number and wide range of thermodynamic variables such as pressure and temperature. The purpose of this study is to investigate fluid flow and heat transfer coefficient distribution of supercritical water in a tube using numerical simulation. The results could be used in design and fundamental analysis of heat exchanger systems which use fluids under the supercritical state.

2. Numerical modeling

2.1 Governing equations and boundary conditions

The problem considered here is laminar convective heat transfer at zero gravity to water under the supercritical state flowing through a smooth circular tube with a constant wall heat flux. Flow is assumed to be steady state and axisymmetric. And local thermodynamic equilibrium with Newtonian fluid is also assumed. The governing continuity, Navier-Stokes, and energy equations in axisymmetric coordinates, which are used in this modeling are shown as following,

Continuity :

$$\frac{1}{r}\frac{\partial}{\partial r}(\rho r v)+\frac{\partial}{\partial z}(\rho u)=0 \tag{1}$$

Momentum :

$$\rho v\frac{\partial v}{\partial r}+\rho u\frac{\partial v}{\partial z}=-\frac{\partial P}{\partial r}+\frac{1}{r}(r\tau_{rr})-\frac{\tau_{\theta\theta}}{r}+\frac{\partial}{\partial z}(\tau_{rz}) \tag{2}$$

$$\rho v\frac{\partial u}{\partial r}+\rho u\frac{\partial u}{\partial z}=-\frac{\partial P}{\partial z}+\frac{1}{r}(r\tau_{rz})+\frac{\partial}{\partial z}(\tau_{zz}) \tag{3}$$

where,

$$\tau_{rr} = \mu\left[2\frac{\partial v}{\partial r} - \frac{2}{3}(\nabla \cdot V)\right] \quad (4)$$

$$\tau_{\theta\theta} = \mu\left[2\frac{v}{r} - \frac{2}{3}(\nabla \cdot V)\right] \quad (5)$$

$$\tau_{zz} = \mu\left[2\frac{\partial u}{\partial z} - \frac{2}{3}(\nabla \cdot V)\right] \quad (6)$$

$$\tau_{rz} = \mu\left(\frac{\partial u}{\partial r} + \frac{\partial v}{\partial z}\right) \quad (7)$$

Energy :

$$\rho C_p \frac{DT}{Dt} = Div(k\nabla T) + \beta T\frac{DP}{Dt} + \mu\Phi \quad (8)$$

Flow enters the tube with fully developed velocity and uniform temperature. At the wall constant heat flux boundary condition is applied and symmetry is used at the centerline of the tube. At the outlet, which is placed 50~100 diameters downstream of the tube inlet, dependent variables of fluid velocities and temperature are linearly extrapolated to provide the axial downstream conditions. The effect of the extrapolation boundary conditions are checked by comparison with the simulation results of longer tube. Thermophysical properties of water are taken to be functions of temperature and pressure with the assumption of thermodynamic equilibrium. For the properties the computer code of Lester et al.[1] is used.

2.2 Solution procedure

The governing equations of continuity, momentum, and energy are solved with the SIMPLE algorithm using second order upwind scheme. A staggered grid system is used and relaxation factors are used for stability. The convergence is checked by computing the normalized residual of the equations. The iteration is stopped when the residual is less than 10^{-3}. All calculations are performed on HP workstation (Model 1100) with Compaq Fortran compiler.

For this numerical calculation an orthogonal non-uniform grid system is used. And grid points are clustered near the wall and entrance where there is large variation in flow and heat transfer variables. For most calculations with $L/D=100$ a grid of 300 (axial)×70 (radial) is applied. Grid dependence of the solution is checked by refining the radial and axial grid system.

3. Results and discussion

3.1 Comparison with other modeling data

Current simulation results are compared with previous modeling data for the variable property case. Figure 2 shows comparison of velocity and temperature distributions in the tube and it can be seen that the two predictions agree well.

3.2 Distributions of fluid velocity, temperature, and properties in the tube

Figures 3~6 show distributions of velocity, temperature, and thermodynamic and transport properties of supercritical water in the tube for various inlet temperatures and pressures. As the fluid temperature increases with heat transfer from the wall through pseudocritical temperature there are severe variations of the thermodynamic and transport properties and they

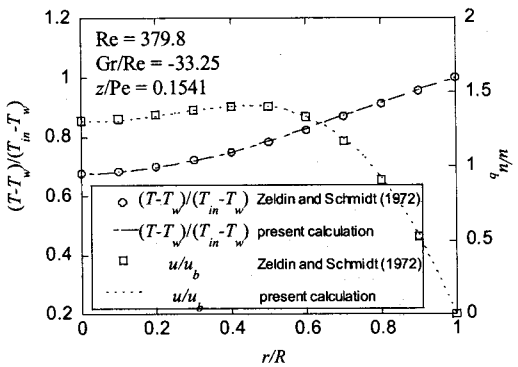

Fig. 2 Comparison of present simulation with other modeling results.

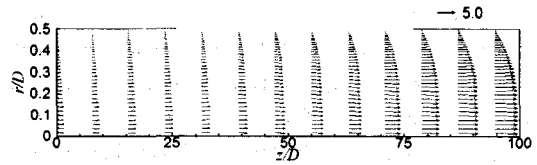

(a) Axial velocity (u/u_{in})

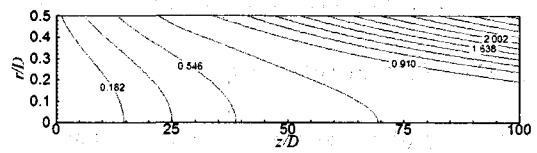

(b) Temperature (T^*)

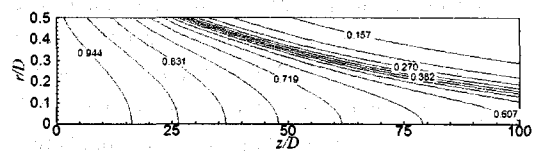

(c) Density (ρ/ρ_{in})

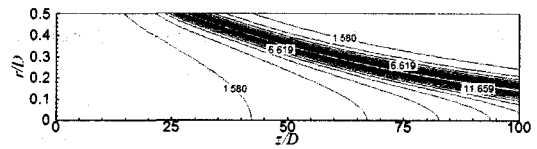

(d) Specific heat ($C_p/(C_p)_{in}$)

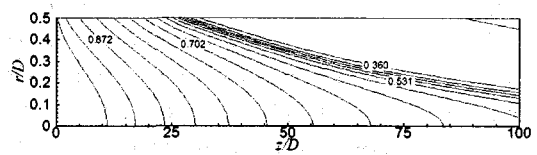

(e) Viscosity (μ/μ_{in})

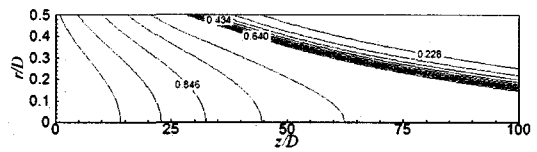

(f) Thermal conductivity (κ/κ_{in})

Fig. 3 Distributions of nondimensionalized velocity, temperature and properties in the tube for Q_w=5.0 kW/m^2, P_R=1.1, $(T_R)_{in}$=0.9, Re_{in}=200.

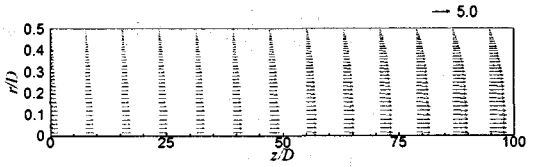

(a) Velocity (u/u_{in})

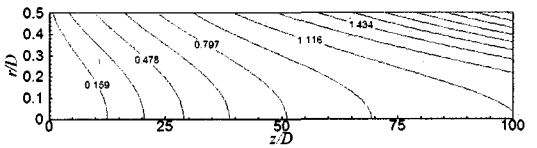

(b) Temperature (T^*)

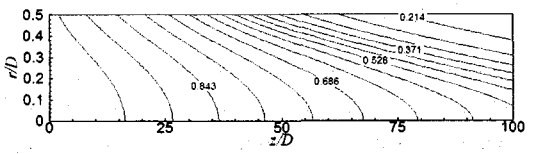

(c) Density (ρ/ρ_{in})

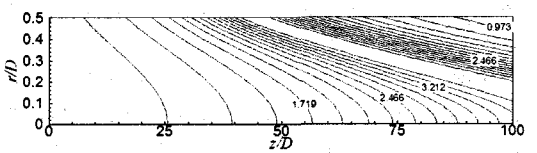

(d) Specific heat ($C_p/(C_p)_{in}$)

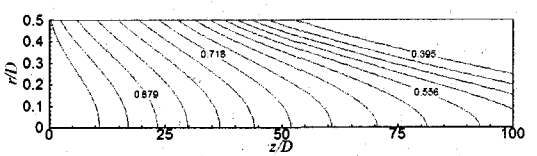

(e) Viscosity (μ/μ_{in})

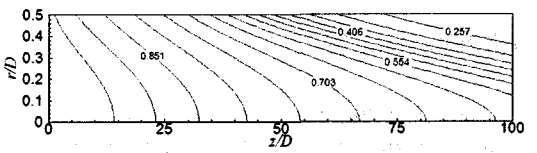

(f) Thermal conductivity (κ/κ_{in})

Fig. 4 Distributions of nondimensionalized velocity, temperature and properties in the tube for Q_w=5.0 kW/m^2, P_R=1.5, $(T_R)_{in}$=0.9, Re_{in}=200.

affect fluid flow and heat transfer in the tube as shown in Fig. 3. Flow accelerates along the tube because of the decrease of fluid density caused by the increase of fluid temperature due to heat transfer from the wall. As in the density distribution the flow acceleration becomes

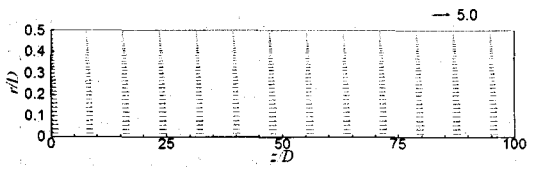

(a) Axial velocity (u/u_{in})

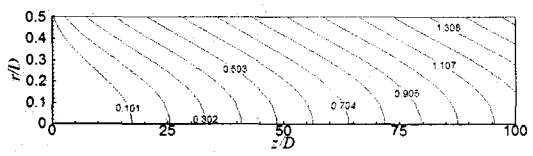

(b) Temperature (T^*)

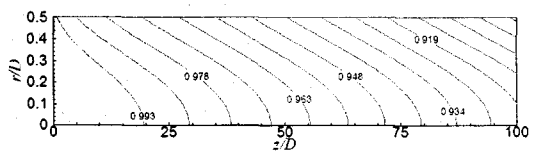

(c) Density (ρ/ρ_{in})

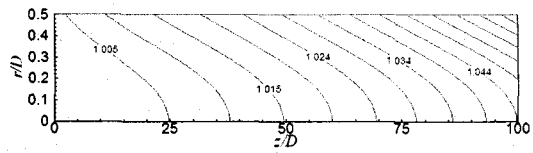

(d) Specific heat ($C_p/(C_p)_{in}$)

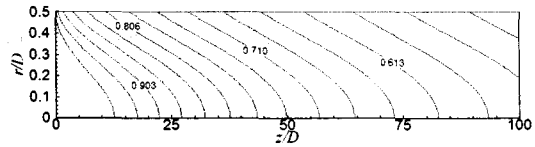

(e) Viscosity (μ/μ_{in})

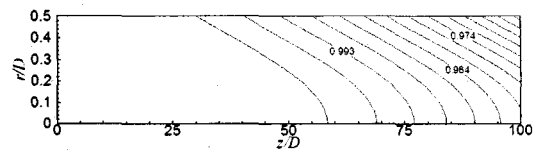

(f) Thermal conductivity (κ/κ_{in})

Fig. 5 Distributions of nondimensionalized velocity, temperature and properties in the tube for Q_w=5.0 kW/m^2, P_R=1.1, $(T_R)_{in}$=0.6, Re_{in}=200.

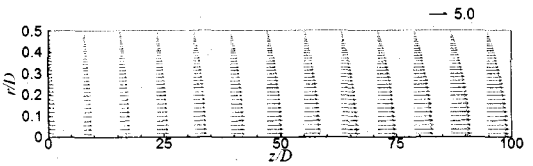

(a) Axial velocity (u/u_{in})

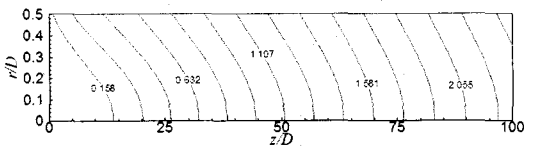

(b) Temperature (T^*)

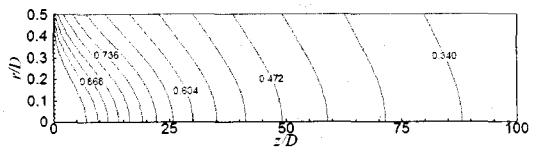

(c) Density (ρ/ρ_{in})

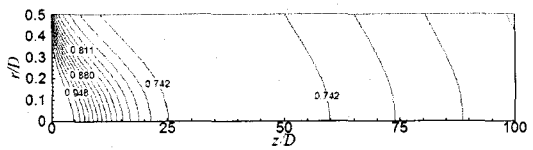

(d) Specific heat ($C_p/(C_p)_{in}$)

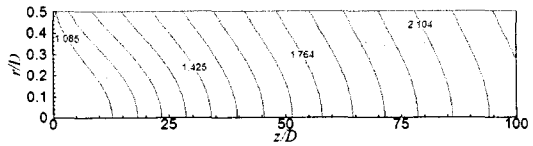

(e) Viscosity (μ/μ_{in})

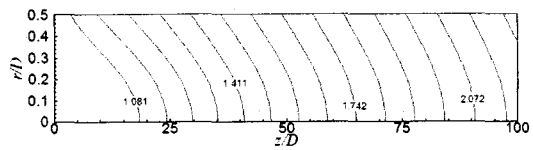

(f) Thermal conductivity (κ/κ_{in})

Fig. 6 Distributions of nondimensionalized velocity, temperature and properties in the tube for Q_w=5.0 kW/m^2, P_R=1.1, $(T_R)_{in}$=1.2, Re_{in}=200.

remarkable when the pseudocritical temperature is between centerline and wall of the tube. And radial gradient of fluid velocity near the centerline ($r/D \leqq 0.2$) becomes flatter in the downstream region of $z/D \geqq 50$.

It can be seen that the pseudocritical tem-

perature region moves to the centerline of the tube and the properties of density, viscosity, and thermal conductivity have similar distributions in the tube as shown in Fig. 1. Specific heat has about 2 times higher order of variation in the tube and there is a steep peak region ($z/D \geqq 30$) at the pseudocritical temperature. There is also smaller peak of thermal conductivity in that region. Radial variation of axial fluid velocity in the tube is not severe in comparison with the steep variation of the properties. Temperature gradient increases remarkably near the region of pseudocritical temperature. It is due to transition behavior of thermal conductivity between liquid-like and gas-like phases.

In Fig. 4 pressure in the tube is increased to $P_R=1.5$. Pseudocritical specific heat in this pressure is about 1/4 of that in $P_R=1.1$ and variation of other properties near the pseudocritical temperature is not so severe. Hence the properties variation in the flow field is relatively not steep. The pseudocritical temperature region in the tube moves to downstream of $\triangle(z/D)\cong 20$ since pseudocritical temperature is increased by nearly 30 K. Flow acceleration along the tube and temperature gradient are a little reduced, and fluid velocity at the outlet is decreased by about 30% compared with Fig. 3.

Figure 5 shows results of the case in which bulk fluid temperature in the tube does not reach pseudocritical temperature, $(T_R)_{pc}=1.01$ with much lower inlet temperature of $T_R=0.6$. Flow acceleration in axial direction is almost negligible and most of the fluid properties have uniform distributions in the tube although there is a little variation of viscosity near the entrance of the tube. So the distributions of fluid velocity and temperature are not much different from those of constant property flow case.

Results of the case where fluid temperature at the inlet of the tube is higher than the pseudocritical temperature are shown in Fig. 6. Fluid properties of density, viscosity, and thermal conductivity at the inlet are reduced to 1/3 ~1/6 of those for the case of $T_R=0.6$ and the fluid has the characteristics of gas-like phase on the whole. Fluid velocity gradient near the centerline increases along the tube with flow acceleration unlike the case of $T_R=0.9$. This difference in fluid velocity distributions is caused by the local phase transition-like behavior of fluid density and viscosity in the case of $T_R=0.9$ while flow acceleration appears in both cases because of density decrease. Increase rate of fluid temperature at the centerline and temperature gradient at the wall are quite different compared with the cases of $T_R=$ 0.6 and 0.9. Near the entrance of the tube there are large variations of density and specific heat. Other properties also have gradual variation along the tube even if it is not locally steep in the flow. Hence it can be said that the case of Fig. 3 is intermediate condition of Figs. 5~6 while there are large differences in the distributions of fluid velocity and temperature because of local steep variation of properties near the pseudocritical point.

3.3 Heat transfer coefficient distribution along the tube

Figures 7~8 show heat transfer coefficient distributions for various inlet temperatures and pressures in the tube. It can be seen that heat transfer coefficient decreases very rapidly near the entrance region and starts to increase as fluid temperature approaches to the pseudocritical temperature. When the bulk temperature of water is about 15 K below the pseudocritical temperature the heat transfer coefficient reaches a peak and then decreases again. This anomalous increase of heat transfer coefficient is due to high specific heat and thermal conductivity near the pseudocritical temperature. As shown in Fig. 7 the peak in heat transfer coefficient distribution increases as pressure in the tube approaches to the critical pressure. The

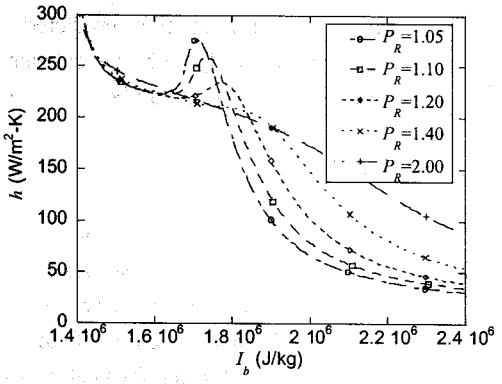

Fig. 7 Comparison of heat transfer coefficient distributions with various pressures in the tube; Q_w=5.0 kW/m^2, Re_{in}=200, $(T_R)_{in}$=0.9.

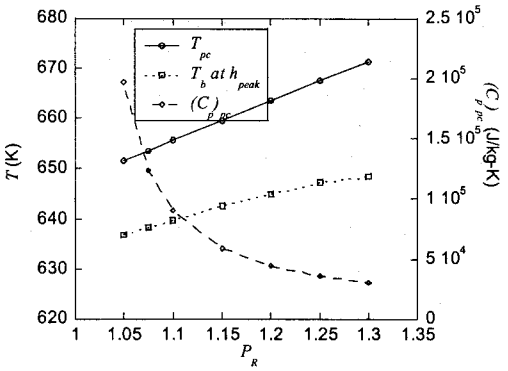

Fig. 9 Bulk temperature at h_{peak} and pseudo-critical temperature with specific heat for various pressures; Q_w=5.0 kW/m^2.

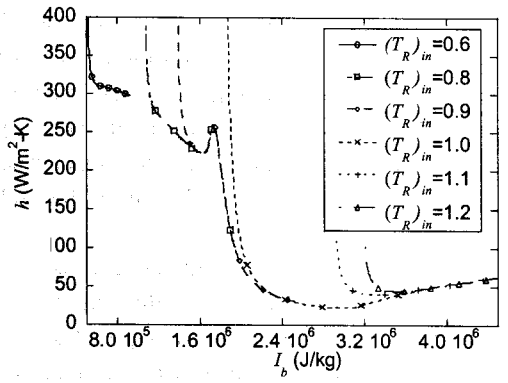

Fig. 8 Comparison of heat transfer coefficient distributions with various inlet water temperatures; Q_w=5.0 kW/m^2, Re_{in}=200, P_R=0.9.

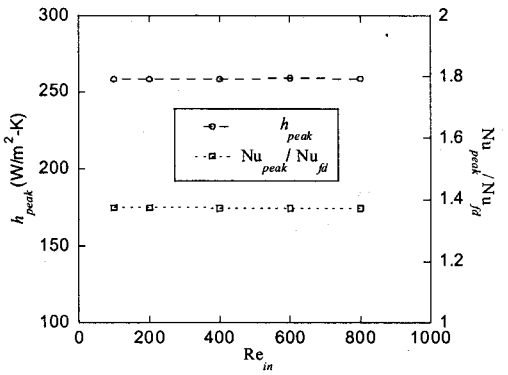

Fig. 10 Peaks of heat transfer coefficient and Nusselt number for various inlet Reynolds numbers; Q_w=5.0 kW/m^2, P_R=0.9, $(T_R)_{in}$=0.9.

axial location of the peak moves to upstream because of pseudocritical temperature decrease with the decrease of pressure. Heat transfer coefficient distribution near the entrance of the tube is affected by inlet temperature, and far from the entrance region it shows a specific distribution characteristic along the tube with bulk fluid enthalpy as in Fig. 8. Especially the peak of heat transfer coefficient is little influenced by inlet temperature, and heat transfer coefficient decreases rapidly to about 1/8 through pseudocritical point due to the transition characteristics between liquid-like and gas-like phases of fluid properties.

Figure 9 shows bulk temperature at h_{peak} and pseudocritical temperature with specific heat for various pressures. Pseudocritical temperature increases almost linearly with the increase of pressure and specific heat at the pseudocritical point decreases very rapidly as pressure is in the proximity of critical pressure. Bulk temperature at the peak of heat transfer coefficient also increases with the increase of pressure and difference between pseudocritical and bulk

temperatures increases from 15 K at P_R=1.05 to 23 K at P_R=1.3. Effect of inlet Reynolds number on the peak of heat transfer coefficient and Nusselt number is shown in Fig. 10 where Nu_{fd} is the Nusselt number of thermally fully-developed flow with uniform fluid properties. It can be seen that they are little influenced by the inlet Reynolds number.

Variation of Nusselt number peak with respect to pressure for several heat fluxes from the tube wall is shown in Fig. 11. The peak of Nusselt number increases as the pressure in the tube approaches to the critical pressure. It is caused by the rapid increase of peak values of specific heat and thermal conductivity at the pseudocritical temperature while the effect of thermal conductivity is relatively small. The peak also increases with the decrease of heat flux from the wall and the effect of wall heat flux is not so remarkable for pressure higher than P_R=1.40.

From the simulation results the Nusselt number peak can be correlated as following equation with consideration of various parameters,

$$\frac{Nu_{peak}}{Nu_{fd}} = \frac{0.729}{(P_R-1)^{0.136}\left(\frac{Q_w}{GI_c}\right)^{0.046}} \quad (9)$$

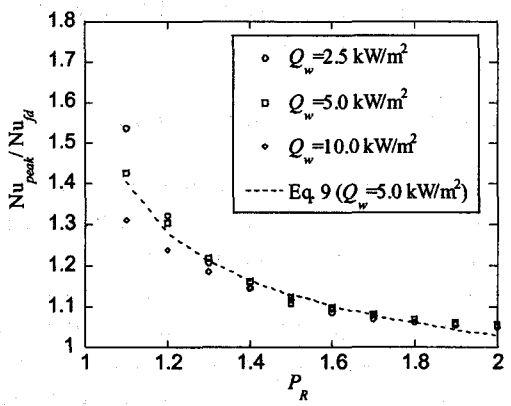

Fig. 11 Variation of Nusselt number peak in the tube with pressure for several wall heat fluxes.

It can be seen in Fig. 11 that predicted results by Eq. (9) agree well with the calculation data for the peak of Nusselt number.

4. Conclusions

Numerical analysis has been carried out to investigate laminar convective heat transfer of supercritical water under zero gravity condition in the tube. The characteristics of fluid flow and heat transfer with thermophysical properties variation in the tube are analyzed for various wall heat fluxes and inlet parameters such as temperature, pressure, and Reynolds number. Following conclusions can be drawn from the numerical results in this study,

(1) There is flow acceleration along the tube and large increase of temperature gradient through the boundary region of pseudocritical temperature with steep variation of thermodynamic and transport properties for supercritical water with constant heat flux from the tube wall.

(2) Heat transfer coefficient has a peak when bulk fluid temperature is less than pseudocritical temperature (about 10 K for Q_w=5.0 kW/m^2) and temperature difference between bulk and pseudocritical temperatures decreases as the pressure in the tube approaches the critical pressure.

(3) The peak of heat transfer coefficient near the pseudocritical point is largely influenced by pressure and wall heat flux rather than Reynolds number and temperature at the tube inlet. Following correlation to predict the peak of Nusselt number is suggested,

$$\frac{Nu_{peak}}{Nu_{fd}} = \frac{0.729}{(P_R-1)^{0.136}\left(\frac{Q_w}{GI_c}\right)^{0.046}}$$

In this numerical study water is used as a fluid under the supercritical state. More specific analyses on the interrelations of heat transfer

parameters need to be carried out for various supercritical fluids in order to understand fundamental heat transfer mechanism near the thermodynamic critical point.

References

1. Lester, H., John, S. G. and George, S. K., 1984, Steam Tables, Hemisphere, New York.
2. Hendricks, R. C., Simoneau, R. J. and Smith, R. V., 1970, Survey of Heat Transfer to Near Critical Fluids, NASA Technical Note, TN-D5886.
3. Hall, W. B., 1971, Heat transfer near the critical point, Advances in Heat Transfer, Vol. 7, pp. 1-83.
4. Polyakov, A. F., 1991, Heat transfer under supercritical pressures, Advances in Heat Transfer, Vol. 21, pp. 1-53.
5. Choi, Y. D., Joo, K. S., Kim, Y. C. and Kim, M. S., 2002, Numerical analysis of turbulent carbon dioxide flow and heat transfer under supercritical state in a straight duct with a square cross-section, Korean Journal of Air-Conditioning and Refrigeration Engineering, Vol. 14, No. 12, pp. 1004-1013.
6. Lim, H. Y., Choi, Y. D., Kim, Y. C. and Kim, M. S., 2003, Development of a new correlation for the heat transfer coefficient of turbulent supercritical carbon dioxide flow, Korean Journal of Air-Conditioning and Refrigeration Engineering, Vol. 15, No. 4, pp. 274-286.
7. Li, L. J., Lin, C. X. and Ebadian, M. A., 1999, Turbulent heat transfer to near-critical water in a heated curved pipe under the conditions of mixed convection, International Journal of Heat and Mass Transfer, Vol. 42, No. 16, pp. 3147-3158.
8. Lee, S. H. and Howell, J. R., 1999, Convective heat transfer in the entrance region of a vertical tube for water near the thermodynamic critical point, International Journal of Heat and Mass Transfer, Vol. 42, No. 7, pp. 1177-1187.
9. Zhou, N. and Krishnan, A., 1995, Laminar and turbulent heat transfer in flow of supercritical CO_2, 30th National Heat Transfer Conference, Portland, pp. 53-63.
10. Kurganov, V. A. and Kaptilnyi, A. G., 1993, Flow structure and turbulent transport of a supercritical pressure fluid in a vertical heated tube under the conditions of mixed convection experimental data, International Journal of Heat and Mass Transfer, Vol. 36, No. 13, pp. 3383-3392.
11. Olson, D., 1999, Heat transfer in supercritical carbon dioxide with convective boundary conditions, 20th International Congress of Refrigeration, IIR/IIF, Sydney, pp. 1-7.
12. Ghajar, A. I. and Asadi, A., 1986, Improved Forced convective heat transfer correlations for liquids in the near-critical region, AIAA Journal, Vol. 24, No. 12, pp. 2030-2037.
13. Koshizuka, S., Takano, N. and Oka, Y., 1995, Numerical analysis of deterioration phenomena in heat transfer to supercritical water, International Journal of Heat and Mass Transfer, Vol. 38, No. 16, pp. 3077-3084.
14. Popov, V. N. and Valueva, E. P., 1988, Numerical modeling of mixed turbulent convection of helium at supercritical parameters of state in vertical tube, Teploenergetika, Vol. 35, pp. 54-59.
15. Dashevsky, Y. M. and Malkovsky, V. I., 1985, Heat exchange with laminar upflow of supercritical helium in a gravitational field, Cryogenics, Vol. 25, pp. 658-659.
16. Bellmore, C. P. and Reid, R. L., 1983, Numerical prediction of wall temperatures for near-critical para-hydrogen in turbulent upflow inside vertical tubes, Journal of Heat Transfer, Vol. 105, pp. 536-541.
17. Vlakhov, E. S., Mieopol'skii, Z. L. and Khasanov-agaev, L. R., 1981, Heat transfer to a supercritical medium with mixed convection and rising flow in heated tubes, Teploenergetika, Vol. 28, No. 11, pp. 69-71.

18. Shiralkar, B. S. and Griffith, P., 1969, Deterioration in heat transfer to fluids at supercritical pressure and high heat fluxes, Journal of Heat Transfer, Vol. 91, No. 1, pp. 27-36.
19. Shitsman, M. E., 1968, Impairment of the heat transmission at supercritical pressures Teploenergetika, Vol. 15, pp. 57-61.
20. Zeldin, B. and Schmidt, F. W., 1972, Developing flow with combined forced-free convection in an isothermal vertical tube, Journal of Heat Transfer, Vol. 94, pp. 211-223.